Friction and Dissipation in Surfaces Functionalized by Organic Monomolecular Assemblies

S. K. Biswas

Abstract | That organic monolayers provide protection to surfaces in contact and in relative motion is recognized in a wide range of applications; from artificial human joints to micromachines to automobile engines. The contact configurations and tractions in these applications vary over a span of many orders of length scales and pressures respectively. In this essay we first review past works to explore the validity of basic laws of friction over these spans of length scale and pressure and demonstrate this validity for two practical systems; silanes on aluminium and silicon, and fatty acids on steel. Such validity provides a means for design of microelectro-mechanical systems as much as it provides a rationale for design and selection of boundary lubricants in large machineries. Our present understanding of the genesis of friction in self assembled monolayers is reviewed next. Application of traction to these monolayers generates translational and rotational motions at the level of chemical bonds which disturb the crystallographic symmetries and generates disorder. On unloading these stored energies are dissipated. The more the avenues of energy dissipation higher is the frictional resistances. The frictional work equilibrates with the total energy that can be dissipated. We review the experimental and theoretical basis of this understanding and explore the dissipation mechanism experimentally. We conclude that translational motion, initiated almost instantaneously on contact, is purely elastic in character and consists of collective tilt and bending of molecular backbones accompanied by bond stretching. This is followed by viscoelastic rotational motions which generate gauche defects. The latter process is only partially reversible. The latter introduces a time element into the frictional response which we demonstrate is related to the ratio of contact intermittency which is a function of velocity and stroke length and relaxation time which is a function of the applied pressure and the molecular configuration of the monolayer.

Mechanical Engineering Department, Indian Institute of Science, Bangalore 560012, India.
skbis@mecheng.iisc.ernet.in

Micromachine: For example, machines incorporating spur gears of 100μm pitch diameter; electric motors, gas turbines, nozzles, pumps, valves, switches, optoelectronic devices with dimensions in the range of two to few thousand micrometers.

Micro-electro-mechanical systems (MEMS): The systems are made of silicon and, more recently non silicon materials, fabricated by photolithographic and micromachining processes. For example; pressure and chemical sensors, linear and rotary actuators.

Introduction

Today a variety of human concerns emerging from diverse avenues of endeavour demand a reduction in friction when two bodies in contact move relative to each other. The concern stems from, to give a few examples, artificial human joints, micromachines and micro-electro-mechanical systems, mining of natural resources, manufacturing and transportation. Miniaturisation of machines poses the problem of stiction. If Amonton's law

is valid the coefficient of friction is independent of contact area. The availability of inertial force required to overcome this universal friction is a challenge to ensure continuous efficient motion in micromachines. In large machineries such as in internal combustion engines, acute global competition demands a decrease in frictional resistance in the cylinder to improve efficiency. There is a related problem to minimise dissipation to prolong the intervals of oil change. Other issues, which dominate technological choices today are safety, environment and ecology. New tribological materials have a major role to play as conventional tribological materials are non-biodegradable. A search for ashless fuels and lubricants provide a new drive for tribological research. The power transmission to weight ratio as well as life continues to be challenges in design of machineries. With phenomenal advances in materials science and technology in the last decade or so radically new materials solutions are becoming practical technologies. These include alloys with memory, alloys with property gradients, monolithic and multilayered coatings, nano particles, often made from new materials and synthesized by novel processing techniques. To achieve multifunctionality conventional metals, ceramics and polymers are synthesized together into composites. New materials are generally lighter, structurally stronger, and have enhanced optical, electrical and thermal properties. To suit a set of exclusive functionalities appropriate for an application today one is able to choose an appropriate combination from a vast array of available materials and processing techniques.

While the above shows a giant stride forward in technology, the stride has brought with it generic problems such as friction. The technological functionalities are rarely inclusive of tribology. Tribology therefore becomes a problem which needs to be solved abinitio given apriori the materials, load, velocity and the environment. Research and development works on polymer brushes for human replacement joints; additives for aluminium and magnesium substrates in new light weight engine bores with new surface textures; and lubricants for a new generation of electronic components and structural materials to be used in storage devices and micromachines, are therefore of much current interest. The complexity of problems faced by tribologists today is high and there is a widespread belief in this community that solutions are not simply incremental and there is a genuine need to revisit the basics in order to equip this and the next generation of practitioners with tools adequate to face the new challenge.

In this essay we first revisit the basic law of friction to understand the universality or lack of it when used to describe phenomena over many orders of length scales and diverse surface topology and chemistry. The initial part of this essay is much inspired by the reflections and works of Prof. U. Landman of Georgia Institute of Technology, US, and Prof. J. Israelachvili of University of California, Santa Barbara, US. In the second part we will examine data from our work carried out at the Indian Institute of Science which focuses on the validity of performance differential which exists in the tribology of: (1) two chemically and structurally distinctive boundary lubricant molecules and (2) two chemically identical but physically distinct, additive molecules over many order of length scales. We will finally discuss possible dissipation mechanisms when monolayers of the above test additives self assembled on a variety of substrate are slid against a rigid probe.

Figure 1: A schematic of change in friction force and contact area under different contact conditions, summarized from the SFA experimental results given in ref (5).

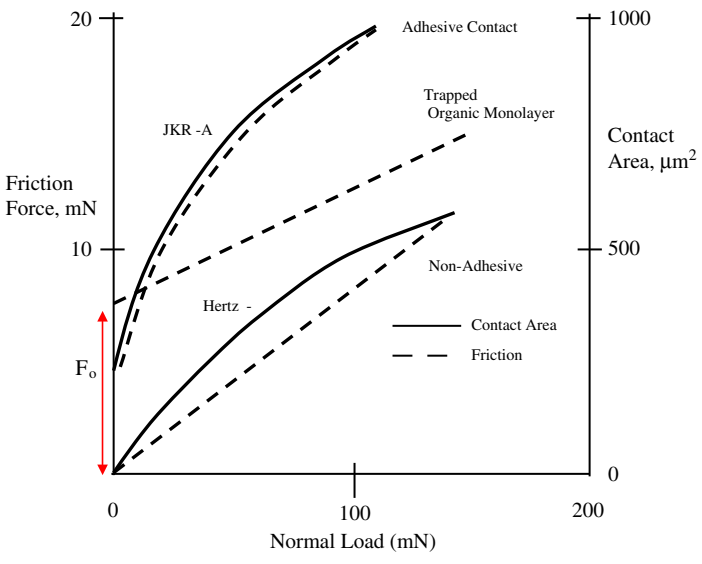

Laws of Friction

From very early times (≈3000 BC onwards) human kind have optimized mechanical systems to minimise the force required to institute relative motion. To push and pull large blocks of building material against the ground, the invariance of coefficient friction with contact area was used by the Egyptians, and Indians in Mohanjadaro and Harappa. The advantage of transportation by waterways was preferred by the Mesopotamian and Harappans to take advantage of the low shear

Figure 2: Lateral force (0% RH) measured in AFM sliding a silicon nitride tip on octyltrichlorosilane (OTS) monolayer self assembled on aluminium. The results show the characteristics corresponding to a monolayer heat treated to a peak temperature of 483 K and cooled back to room temperature and that corresponding to a non-heat treated monolayer.

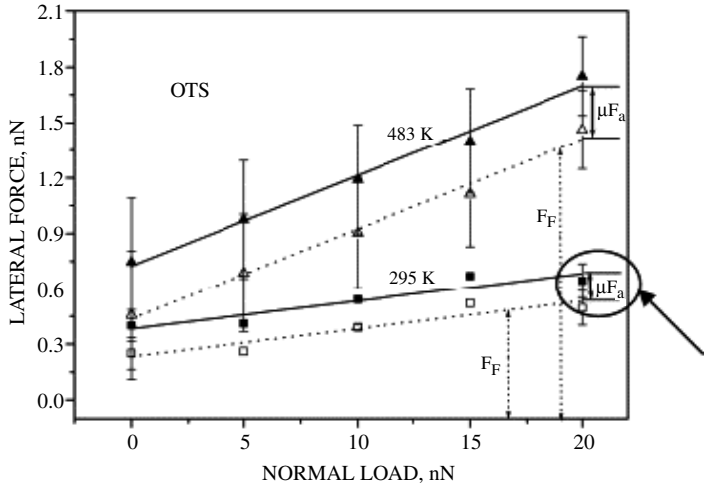

Amonton's Law: Friction is proportional to the applied normal force. Friction is independent of the (apparent) contact area. Sliding friction is independent of the sliding velocity.

Coefficient of friction: Friction force normalized by the applied normal force on a contact.

Hertzian Contact: The circular contact generated by two normally loaded smooth spheres (radius, R_1 and R_2) pressing against each other. The response is elastic and the contact is frictionless. The contact radius; $a = \left((3/4)\frac{LR}{E*}\right)^{1/3}$ where $R = \frac{1}{R_1} + \frac{1}{R_2}$ and $E*$ is the reduced modulus.

Surface Force Apparatus: The instrument measures intermolecular and surface forces between two mica surfaces, the displacement and contact deformation is measured optically. It is used extensively for studying rheology of molecularly thick liquid films.

stresses in water. Pulleys on a shaft were lubricated by animal fat (Arthasastras, 2^{nd} Century BC) to transfer the shear planes to grease and the advantage of rolling contact over sliding contact to minimise friction was realized by all the river valley civilizations as they developed bullock carts, chariots and other modes of ground transport. Such knowledge and understanding, arrived at thorough practice were bound to get systemized into laws through experimentation sooner or later. The first (recorded) known study of friction is due to Leonardo de Vinci (1452–1519 AD) who observed:

1. The proportional increase in friction force with normal load and
2. The friction force is independent of the area of contact.

More detailed experimentation in France and Germany in the 17^{th} and 18^{th} century led to the formulation of what is known as the Amonton's law. A term 'coefficient of friction' was designated as

$$\mu = \frac{F}{L} = \text{Constant} \tag{1}$$

where F is the friction force and L is the normal load. The coefficient of friction, μ is independent of the area of contact, A, and the velocity of sliding, v.

The justification of the law comes from the 'cobble stone' description of a solid surface. An asperity climbs over another which bears an angle θ to a base plane. The resistance to such a climb by an asperity normally loaded (L) is $L\tan\theta$. If there are 'n' such asperities.

$$F = \sum_{i=1}^{n} F_i = \sum_{i=1}^{n} L_i \tan\theta_i = <\tan\theta_i> L = \mu L. \tag{2}$$

The main problem with this formulation, as pointed out by the English engineer Leslie[1] is that once over the hill, the work done to push the asperity up is recovered and continuous application of tangential force is not required to maintain the sliding motion. The work done to cause sliding thus has to be dissipated and this led to many suggestions as to how this may be done to account for the perpetual application of the tangential force to maintain sliding.

Bowden and Tabor[2] in the 1960s proposed that asperities in contact plastically deform and form junctions. The plastic work is dissipated as heat creating a need for subsequent work to be done to keep the surfaces sliding on each other. They assumed the area of contact, A, to be linearly proportional to the applied load, L. As the shear force needed to deform the asperities is proportional to this area, Amonton's law is recovered. A problem arises when the contact is elastic where for a Hertzian contact $A \propto (RL)^{2/3}$ where R is the radius of the sphere pressing a flat counterface. For shear strength of τ_o the friction force $F \propto \tau_o (RL)^{2/3}$, which of course violates Amonton's law. In exploring the applicability of Amonton's law the role of adhesion between the two surfaces was explored next. Derjaguin[3] suggested the inclusion of a molecular force driven overload term L_a, to formulate

$$F = \mu(L_a + L) = F_o + \mu L \tag{3}$$

The formulation opened the way for inclusion of a dissipative term, adhesion hysteresis in the Amonton's law. Molecular level relaxation inherent in deformation by intermolecular forces gives rise to adhesion hysteresis[4]. It also provided a way to include the friction force experimentally observed at $L = 0$ but remained problematic as it gives infinite friction at $L = 0$.

One of the major experimental breakthroughs which emerged from the Cavendish laboratory in England in 1960[2], is the Surface Force Apparatus. The apparatus enables compression and shear of two mica surfaces against each other, but more importantly it provides a measurement of the contact area as it evolves with the application of these forces.

A summary of experimental findings obtained[5] using SFA, for mica surfaces in contact, is given

Figure 3: Temperature dependence of peak frequency for different thermal cycles. (a) CH_2 antisymmetric stretch for OTS SAM on aluminium. Peak temperatures in the cycles are (■) 483 K and (▲) 403 K. (b) CF_2 antisymmetric stretch for FOTS SAM on aluminium. (■) 573 K and (▲) 423 K. Filled symbol is for heating and open symbol is for cooling.

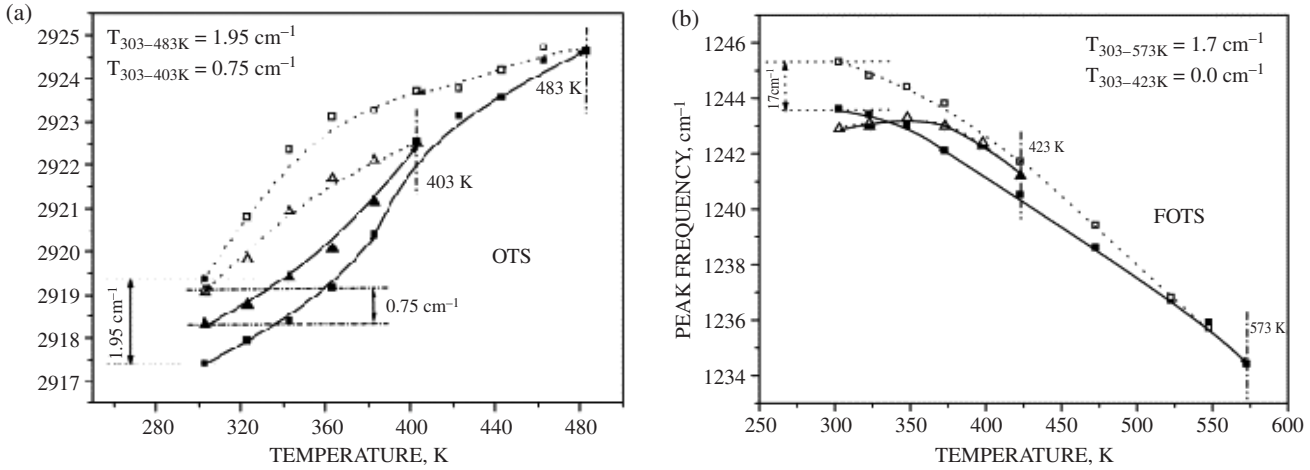

Figure 4: Pull-off force (AFM) at different peak loads in dry air (0% RH) (a) OTS SAM; heat treatment temperatures (■) 295 K and (●) 483 K, (b) FOTS SAM; heat treatment temperatures of (■) 295 K and (●) 573 K and (c) Comparison of mean pull off force for (■) OTS and (▲) FOTS SAM as temperature 295K and same open symbols for heat treatment temperature of 573 K, respectively. The data for OTS at 483 K are not shown due to large scatter in experimental data. Bar shows standard deviation ($\pm\sigma$) of experimental scatter.

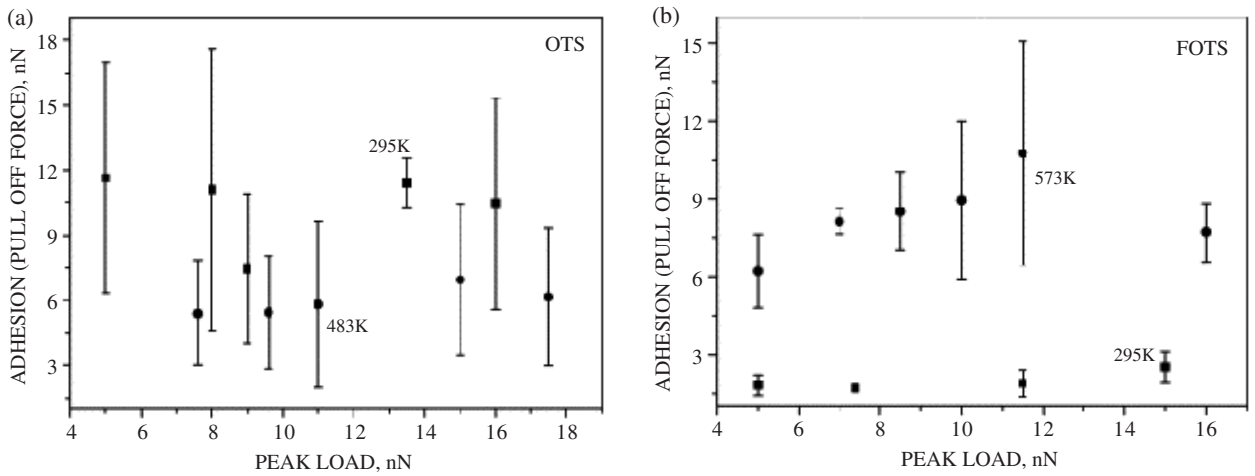

Atomic Force Microscope: The equipment measures forces of interaction between a tip of 10-20 nm radius and sample surfaces. The instrument has the resolution to measure forces in the 10^{-7} to 10^{-9}N range.

in Fig 1. Amonton's law is strictly valid, $F \propto L$, and as $L \to 0, F \to 0$, when the contact is non-adhesive. F here is not proportional to the contact area A which is predictable using Hertzian equations. When the contact is non-lubricated adhesive (as one would achieve under very dry or ultra high vacuum condition), the friction force follows the contact area faithfully. Contact area here can be predicted in this case using the JKR (Johnson, Kendall and Roberts[6]) theory. $A\ L \to 0, A \neq 0$ implies that a tensile force needs to be applied to break the junction (also see[7,8,9]).

Figure 2 shows that when the junction is coated with an organic monolayer there is a finite intercept $F \to F_a$ at $L = 0$ (see eqn. (3)) but otherwise F is linearly proportional to L (also see this trend in[10–15], for a variety of organic molecules assembled on different substrates). Instead of a chemically absorbed monolayer if some fluid such as an alcohol or oil is trapped between the two

Figure 5: (A) Friction forces measured by using the nanotribometer at different loads for (a) OTS SAM after heat treatment, peak temperatures of (■) 295K, (●) 403 K and (▲) 483 K. (b) FOTS SAM after heat treatment, peak temperatures of (■) 295 K, (●) 423 K and (▲) 573 K. (B) Influence of adhesion on lateral force (in dry air, 0% RH); (a) total lateral force due to OTS SAM after heat treatment, temperatures of (■) 295 K and (▲) 573 K and residual friction force indicated by open symbol at same temperatures. Lateral force increases with heat treatment temperature; lateral force due to adhesion also increases with heat treatment temperature.

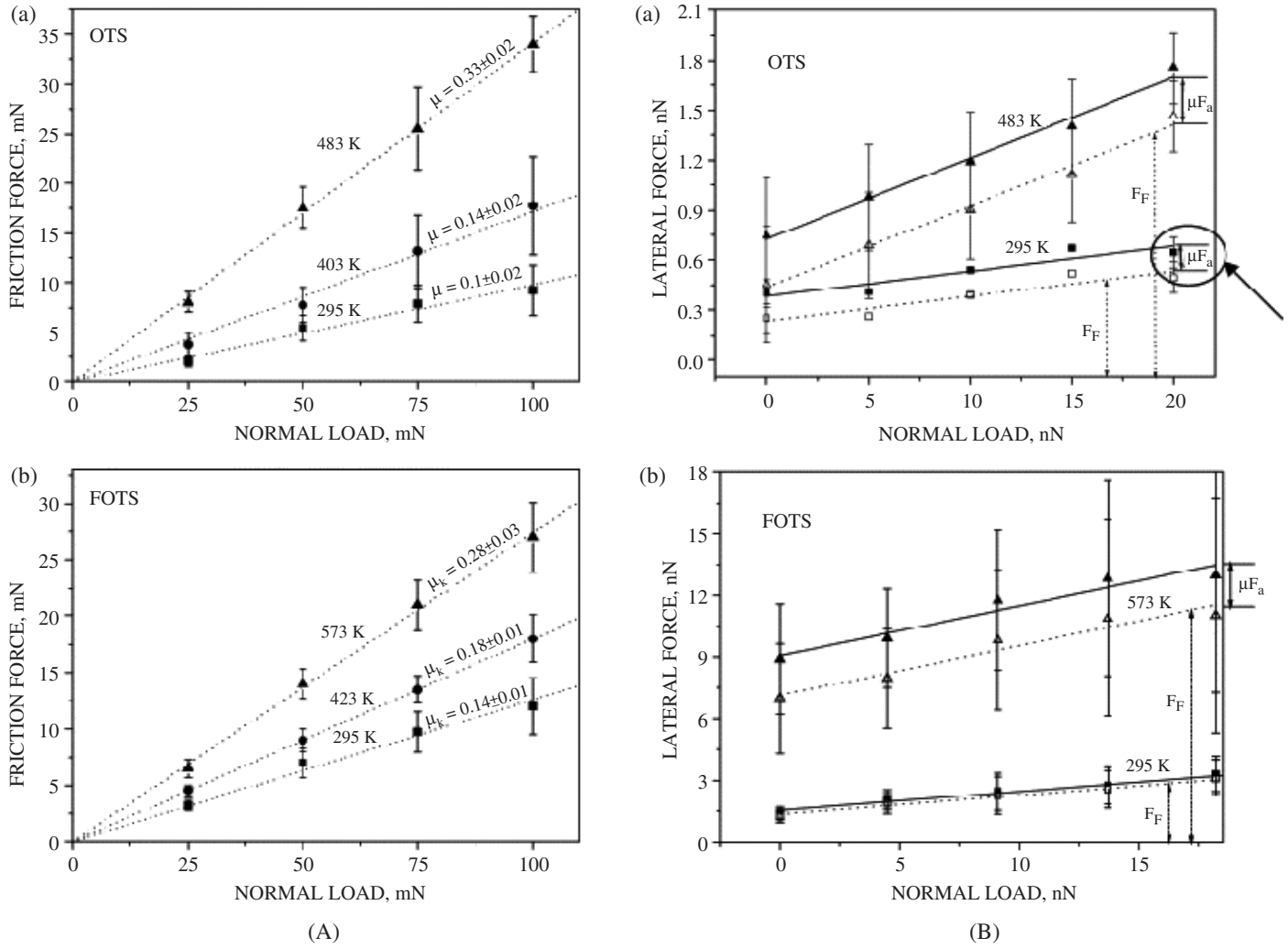

DMT, JKR: The models give the pull off force between two normally loaded elastic spheres in adhesive contact. DMT — Derjaguin, Muller and Toporov — assumes the contact to be defined by Hertzian considerations and adhesive forces to operate outside the contact. JKR — Johnson, Kendall and Roberts — assumes adhesion to exist within the zone of contact and the contact is generated by the applied load and adhesive overload.

surfaces, lateral force measurement in Atomic Force Microscope however show a strict adherence to eqn. (1) $L \to 0$, $F \to 0$. To explore this further, we present below some lateral force measurement done on alkane silane monolayers self assembled on an aluminium surface[16–19]. We heat-treat the monolayer to different temperatures and generate residual molecular disorder which scales with the peak heat-treatment temperature (fig. 3)[20]. The surface free energy of the monolayer increases with peak treatment temperature. Pull-off force measurement shown in fig.4 gives an average value of $F_a = 9nN$ for the adhesive force. Figure 5 shows the lateral force as obtained by sliding a silicon nitride tip on the monolayer. The behaviour is very similar to that shown in fig.1 where smooth mica surfaces were coated with octodecyl phosphonic acid. Assuming that the force of adhesion is independent of normal load (DMT, JKR)[21] we estimate $F_T = F - \mu F_a$ using fig. 4. We note that the friction force F_T (and F) vary linearly with load L, molecular disorder increases μ, and there is a residual friction force at $L = 0$ even after eliminating a possible contribution of the adhesive force. The data presented shows the linear load dependence of friction (eqn. 3) but also points to the state of molecular order which governs avenues of energy dissipation to be an important parameter which determines frictional force as well as coefficient of friction.

Figure 6: Surface free energy of SAMs after heat treatment at different peak temperatures for (■) OTS and (●) FOTS, obtained from contact angle measurements.

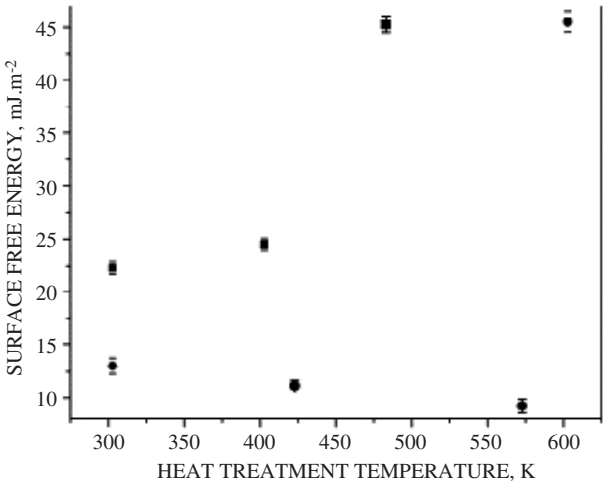

Nanotribology: Study of friction and wear processes ranging from microscopic to atomic level contact.

Nanotribometer: Sliding and reciprocating contact between a pin/ball and a flat surface. The load applied by a piezo actuator varies in the micro-N to N range. The displacement of the levers used to measure friction force is tracked optically. The scale of contact is 1-100 microns.

Macrotribometer: Pin on disc machine; sliding and reciprocating contact. The normal load varies in the 1–200 N range and the scale of contact is mm to cm.

The characteristics shown in fig. 1 may be summarized as follows.

$$F = F_o + \mu L^n \tag{4}$$

- For adhesive two body contact, $F_o \neq 0, n \neq 1$
- For non adhesive two body contact, $F_o = 0, n = 1$
- For adhesive (three body) lubricated contact, $F_o \neq 0, n = 1$

It is clear that Amonton's law (eqn. (1)) is strictly valid for a nonadhesive two body contact, and μ is independent of the load and the area of contact.

For adhesive and lubricated contact the coefficient of friction may be defined as $\mu = \frac{dF}{dL}$. For lubricated contact, μ is a constant, and is independent of load (or area of contact); but for adhesive contact, μ is dependent on the load or the area of contact. Amonton's law is also independent of sliding velocity.

In this paper, we are primarily concerned with friction of functionalized surface or lubricated contact. A validation of the Amonton's law would necessitate a validation of $\mu =$ Constant and independent of load at all loads (contact pressure) and contact areas.

The Scaling Effect

Since the inventions of Atomic Force Microscope and Surface Force Apparatus there has been (as reported above) a flurry of experimental works in the area of nanotribology. This was prompted by the advent of micromachines but also by a desire to explore various asperity, molecular and atomic level mechanisms which had been hypothesized in the past to explain macro-tribological phenomenon but had remained unvalidated due to the lack of microscopic tools. Once it was realized that it is indeed possible to carry out repeatable tribological experiments at the microscopic level, a natural concern expressed was to investigate phenomenological validity across a wide range (of 8–10 orders) of length and pressure scales.

The contact dimension and pressure vary as nm/GPa, 10–100μm/100MPa, 10–100μm/100–1000MPa and mm/1–100MPa in AFM, SFA, nanotribometer and (e.g., pin-on-disc) macrotribometer, respectively. If an identity may be established between the friction characteristics

Figure 7: (a) Coefficient of friction of aluminum against steel pin in presence of OTS and FOTS additives (5% v/v) dispersed in n-hexadecane. (b) Wear measurement of aluminum against steel pin in the presence of OTS and FOTS additives for 250 m sliding distance. Load: 60 N, speed: 0.2m/s.

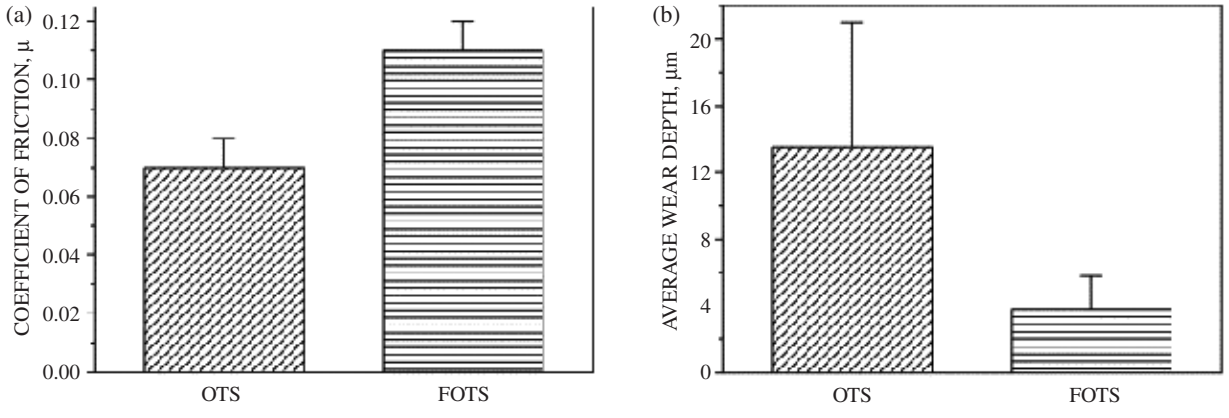

Figure 8: A schematic of the stereic and Linoleic acid structures showing the presence of a double bond in the latter.

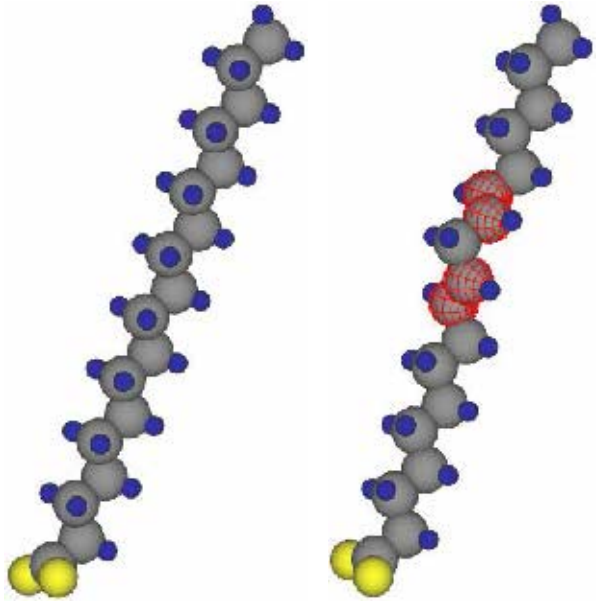

Stearic Acid Linoleic Acid

The molecular conormation and the energy minimized structures of the Stearic and Linoleic Acid, estimated with universal force field. The Carbon atoms are depicted in GRAY, the Hydrogen atoms in BLUE and the Oxygen atoms in YELLOW. The Carbon atoms marked RED are the position of the double bonds.

observed over such a wide scale, it may be possible to extrapolate the molecular level tribophysics and tribochemistry to an industrial application where large scale objects are involved. This, if possible, of course opens up the scope for new approaches in industrial design for optimization of energy and materials.

Two approaches are undertaken to establish this identity. The first one involves simply scaling up an experiment from the AFM to the pin-on-disc level. This is fraught with problems as artificactual machine characteristics such as inertia and resolution interfere with the results. For example, periodic fluctuation in friction force may be due to phase transition in trapped material or related to machine inertia. It may be difficult to distinguish between these two factors. The second approach is to track the differential in performance between two systems over a wide range of length and pressure scales. The latter, while being more immune than the first approach to machine artifact, also provides a bench-top methodology for industrial screening of materials and lubricants.

Gao et al.[5] observed the identity of friction coefficient and F *vs* L characteristics obtained using AFM and SFA over a six order scaling span in contact radius, pressure, load and friction force. This identity was observed for smooth and damaged mica and alumina surfaces under dry, lubricated, adhesive and non-adhesive contacts, the experiments reproducing characteristics very similar to that shown in fig.1. Similar observations have been made by Choi et al.[11] and Ruths et al.[9]. In changing from nN to mN load range, others have, however observed the disappearance of the zero load intercept F_0[14,16,17] and an enhancement of the friction coefficient[16,22]. Figure 5 shows the effects of scaling for two silane monolayers self assembled on aluminium. The absence of F_o term (eqn. (2)) in a large-scale experiment is perhaps not surprising if one considers F_o to be related to JKR and DMT theories is independent of load, pressure, contact radius and material properties ($F_o = 3\pi R\gamma$, where R is the radius of the indentor and γ is the surface energy). It is likely that when the order of friction force is increased by several orders, F_o comes within the resolution of force measurement. For a surface functionalized by organic monolayer the $F - L$ relationship remains strictly linear in all cases over four to eight orders of pressure[5,11,9,14,16,17,22].

Moving on to the second approach to explore the scaling effect Ahn et al.[22] have observed a change in the friction coefficient (0.07–0.08→0.15) brought about by replacing a hydrophobic mono molecular layer (octadecanethiol) by a hydrophilic layer (11-Mercaptondecanoic acid). This difference recorded in an AFM experiment is reproduced in a microtribological experiment (contact radius 14μm, contact pressure 660 MPa). Choi et al.[11] have similarly recorded that the difference between the friction of perfluropolyether and perflurodecyltriethoxysilane self assembled monolayer (SAM) is maintained in changing from AFM experiment (nN) to a mN level tribological experiment.

We have explored[16,17] the perpetuation of an apparent contradiction between the relative magnitude of surface energy and friction of two silane monolayers, over a ten order length scale. Figure 6 shows that a fluorinated silane molecule (FOTS) is consistently less surface energetic than a hydrogenated silane (OTS) monolayer. Figure 5 shows that at the nN and mN levels of load the FOTS SAM however yields a higher level of friction than the OTS SAM. This reversal has been observed by others[10,23,24,25,26]. To take this one step further, fig. 7 shows that when these molecules are dispersed in n-hexadecane and used as a lubricant in a pin-on-disc machine to lubricate

Figure 9: Comparison of friction of stereic and Linoleic acids self assembled on steel. (a) AFM, (b) Nanotribometer (c) Pin-on-disc, additives dispersed (5% v/v) in Hexadecane, load-60 N, speed-0.2 m/s.

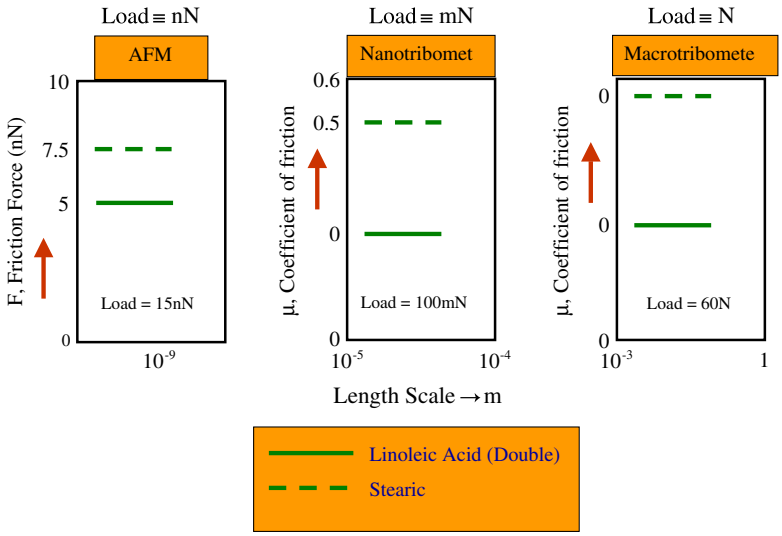

Coefficient of friction for Stearic and Linoleic Acid SAM deposited and dispersed in Hexadecane on steel from Nano to Macro Scale

a steel (pin-3mm diameter) on aluminium contact at a normal load of 60 N and sliding speed of 0.2 m/s, the relative coefficient friction between the two molecules is maintained at this load which is about 10 orders greater than that used in the AFM. Interestingly the wear of aluminium is lower when FOTS molecules are dispersed than when OTS molecules are dispersed in hexadecane.

A similar exercise was undertaken to investigate the effect of a double bond or saturation on the friction of fatty acids self assembled on steel. This effect has been under some debate in the past[27–30]. Figure 8 shows the two chemically and conformationally same molecules, with the stearic acid saturated and linoleic acid unsaturated. Figure 9 shows the comparison of friction recorded in (a) AFM and (b) nanotribometer of both the acids self assembled on a smooth steel surface. Figure 9c shows the comparison when the acids are dispersed in hexadecane and used to lubricate in a pin-on-disc machine. Unsaturation or double bonding is clearly seen in fig.9 to reduce friction at all test-length (contact) scales and pressure regimes.

To summarize the above discussion, we note that experimental results obtained on functionalized surfaces validate Amonton's law, i.e the co-efficient of friction $\mu = \frac{dF}{dL} =$ Constant is independent of load and contact areas at all loads and contact areas achievable in AFM, SFA and nanotribometer experiments. Here the load, contact pressure and contact area varies in a span of eight, two and three orders respectively. What is important is to note that this validity extends over a range of molecular chemistry of the functionalized substance as well as the substrate. Most of the experimental works we have reported have been done on surfaces

Figure 10: (a) Comparison of mean friction coefficient (obtained using a nanotribometer) of OTS and FOTS SAM on aluminium against steel ball after heat treatment, at two different loads. (■) 50 mN and (▲) 100 mN. Speed: 1 mm/s. Filled symbol is for OTS and open symbol is for FOTS SAM. (b) Coefficient of friction recorded for stereic acid (SA) and linoleic acid under two normal loads. It is seen that the friction coefficient of linoleic acid is sensitive to normal load, increasing the normal load from 20mN to 100mN reduces the friction coefficient substantially in that case.

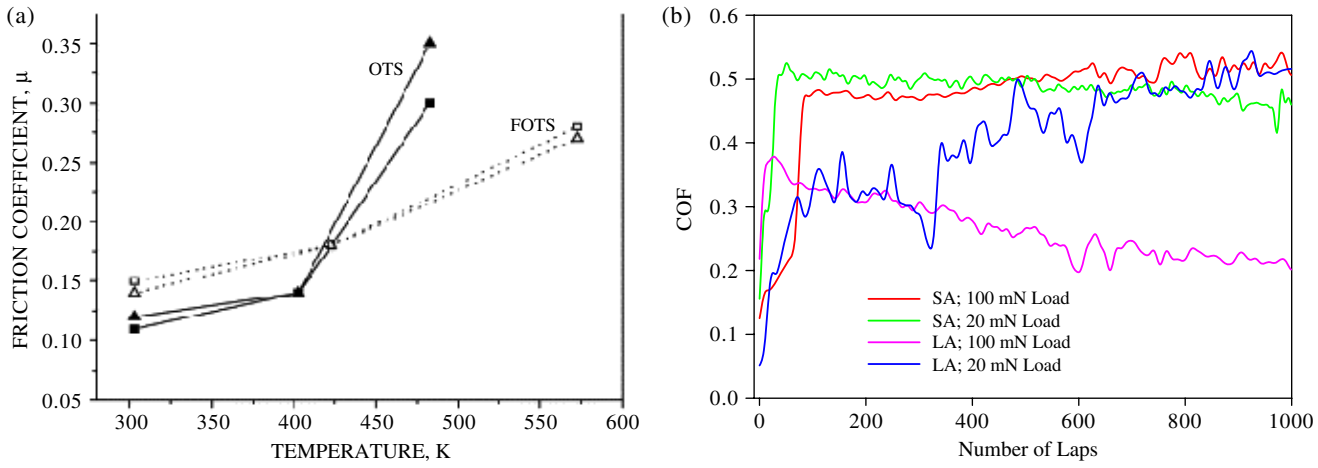

Co-efficient of Friction recorded for Stearic and Linoleic Acid under two normal load

Figure 11: (a) Work done on the system per mole by the probe, estimated knowing the load-displacement characteristics and the volume under real contact area. (b) Estimated confined volume under the real area of contact as a function of applied load.

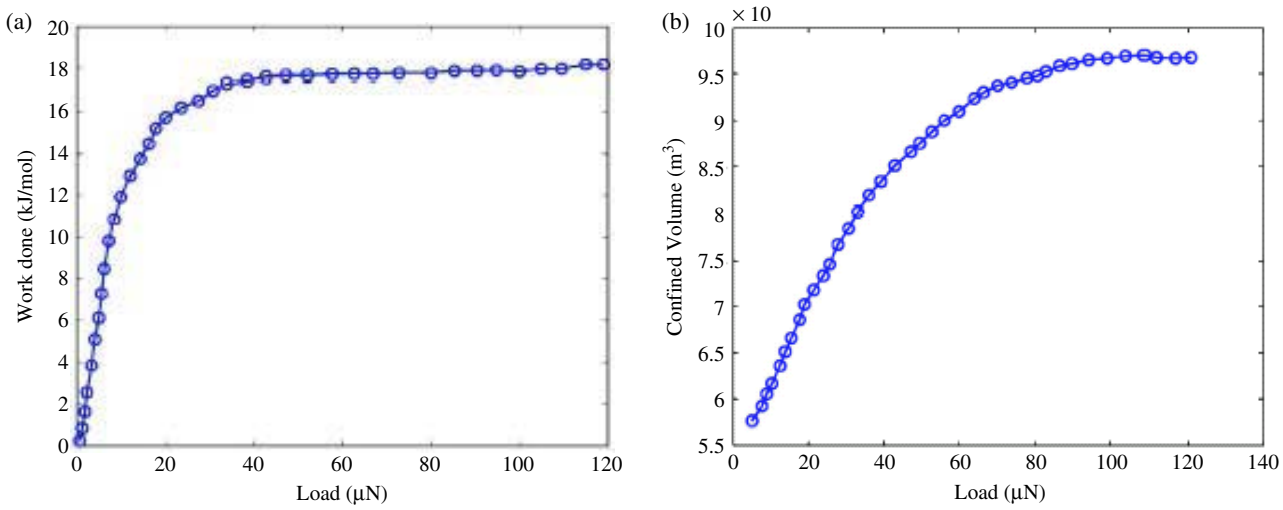

functionalized with crystalline or amorphous monolayers. What is interesting is that the inferences drawn from these works are valid even when the monolayer is highly disordered and liquid like. For example Yoshizawa[4] reports SFA results using hexadecyltrimethylammoniumbromide (CTAB) monolayer which shows $\mu = \frac{dF}{dL} =$ constant and load independent even when the contact area varies nonlinearly as per the JKR model. The *F–L* does not follow the *A–L* characteristics.

We have also demonstrated that the effect of molecular chemistry of the lubricant on friction

XPS (X-ray Photoelectron Spectroscopy): Used for detecting elements and their binding states on a surface. An X-ray photon ionizes the inner level of an atom directly, and the emitted electron is detected.

Figure 12: The relaxation time τ_r the retardation time τ_d, and the stiffness of FOTS SAM as a function of applied load.

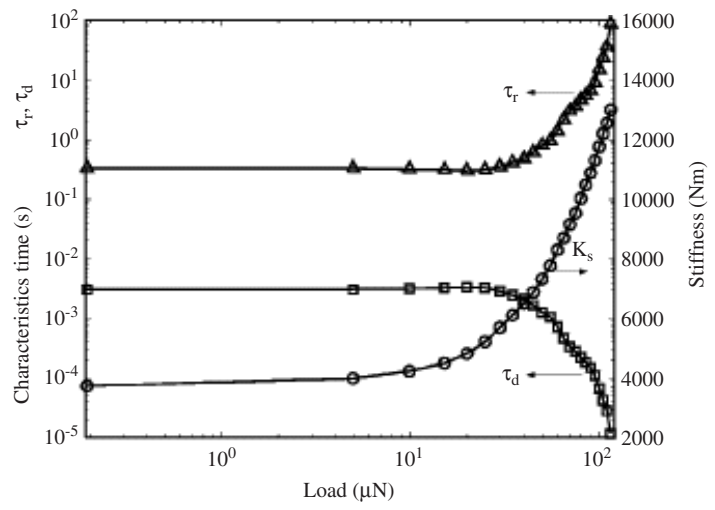

extends over much larger span of load (10 orders) and contact length area (five orders) and appears to be valid even when the molecules are not apriori self assembled but dispersed in a hydrocarbon oil. This implies that the performance of an additive in an industrial machine is ultimately related to its self assembly state on the surface for however brief a time interval. The latter observation must be taken with some caution as there is always a possibility of thermal and pressure activated chemical and physical change specific to a molecule which can alter its relative merit with respect to a more passive molecule substrate interaction. Figure 10 demonstrates two such cases. Figure 10a shows that when the state of disorder brought about by heat treatment is low F_{FOTS} is greater than F_{OTS} but when the disorder is high, F_{OTS} is greater than F_{FOTS}. Figure 10b shows that at low loads the friction of stearic acid and linoleic acid are comparable. At high loads the double bond in linoleic acid brings about a reaction with the steel substrate to form an antifriction salt which lowers its friction coefficient considerably with respect to that of the stearic acid. The phenomenon has been verified using the XPS.

This widespread applicability of Amonton's law over a span of loads, contact areas and materials is indeed curious as especially at larger loads and contact areas the interfaces become more heterogeneous. Enormous chemical, morphological and topographical variations result at the interface in boundary tribology due to statistically distributed roughness; non uniform domains in the monolayers where there is a variation of tilt angles in

Figure 13: The Young's modulus deconvoluted from stiffness data (Fig.12) using Eq. (5) and damping constant to show their opposite trends with load. The inset shows friction coefficient measured for FOTS/Al by a ruby ball under 100 mN normal load. Filled symbols, elastic modulus; unfilled symbols, damping constant. O , FOTS/Al; Δ, FOTS/Si. Arrows show loading direction.

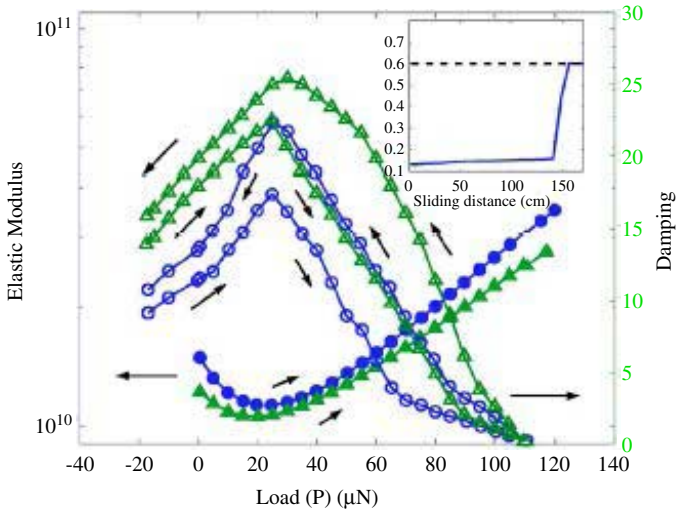

relation to distance from domain boundaries; point and line defects such as domain boundaries in the monolayer; non uniform distribution of contaminants on the substrate surface; the microstructural heterogeneity of the substrate surface itself; presence of environmental water and hydrated monolayers. Gao et al.[5] have addressed this issue using molecular dynamics simulation. Considering the interface as a collection of tiles, they estimated the deformation and friction forces associated with the molecules in each microscopic tile. They observed a large variation in properties associated with the tiles, some well below the time averaged friction force and some well above it. As a matter of fact, they find that at the level of titles the Amonton's law is invalid. However when the average properties over all the tiles are time averaged Amonton's law is recovered. With this tool they are able to, for different interfaces as portrayed in fig. 1, describe the relationship between friction force, contact area and normal load.

Gauche Defect: When mechanical work is done on or heat supplied to molecules, rotational movements take place about the bonds. This takes the molecules out of all-trans configuration. The defects generated thereby are generically known as gauche defects.

Sum Frequency Generation Spectroscopy: A nonlinear optical spectroscopy technique, especially useful for exploring buried interfaces. This is made possible by virtue of the inversion symmetry selection rule, which eliminates the contribution from bulk processes in centrosymmetric materials from the observed signal.

Dissipation

Thermal cycling of SAM

When self assembled organic monolayers are heated or mechanical work is done on them the monolayers are viscoelastically deformed. Heating the monolayer tilts the molecule with respect to an axis normal to the substrate and there is rotation of and about the chemical bonds of the molecules. These deformations are well mapped using vibrational spectroscopy[31–33], x-ray diffraction[34,35] and electro chemical methods[36] for thiol molecules self assembled on gold and silane molecules[37,19]. Molecular dynamic simulation[38,39,40] has corroborated these findings and supported them with subtle explanations. The rotational movements are generally grouped as creating a generic type of defect called the gauche defect. The term arises out of a deviation from all – trans configuration. These defects as they change molecular conformation also change and disturb crystallographic symmetry and cause steric strains. In general, these defects cause molecular disorder. Some of the deformations generated are reversible while others are not. After heating the molecule to a peak temperature if it is cooled back, some of the disorder generated during heating are annealed out but there is residual disorder, which often scale with the peak temperature to which the molecules was heated[37,19,41,42,18].

Compression

Load bearing capacity is an important property of the self assembled monolayers which has a major bearing[22,43,25] on the boundary lubrication tribology of these molecules used as additives. Experiments have been done using AFM and SFA to record the response of these monolayers under compression[45–47]. The initial contact is with the terminal group which enjoys a large degree of freedom of movement and yields a "liquid like" flat response with pressure. The sum frequency generation (SFG) spectroscopic experiments of Salmeron[48] done in tandem with a SFA has clearly shown the bending of the terminal CH_3 stretch mode (alkane silane monolayer) which becomes nearly parallel to the surface, there is an accompanying 120° rotation of this methyl group around the next *C–C* bond axis. This generates gauche defects. As penetration increases, the anchored chains cannot relax and all the adjacent chains pinned in the gap between the indentor and the substrate continue to become compressed against each other and thus reducing the interchain distance with increasing penetration. We note at this stage that the interchain repulsion supports the applied indentation load[45]. A large increase in force is needed to make a very small difference in the interchain distance as well as the confined volume (fig.11). Consequently there is a large increase in stiffness with load[47] as can be seen in fig.12. As the molecules are collectively pressed together, they are likely to constrain each other's movement by interdigitation and entanglement exhibiting a large increase in the relaxation time (fig. 12)[46,47]. Some

Figure 14: Representative vibrational spectra of alkysilane (a) ODTS, (b) DDTS and (c) OTS monolayer deposited on aluminium showing the temperature dependent shifts of methylene antisymmetric (d^-) and symmetric (d^+) stretch modes.

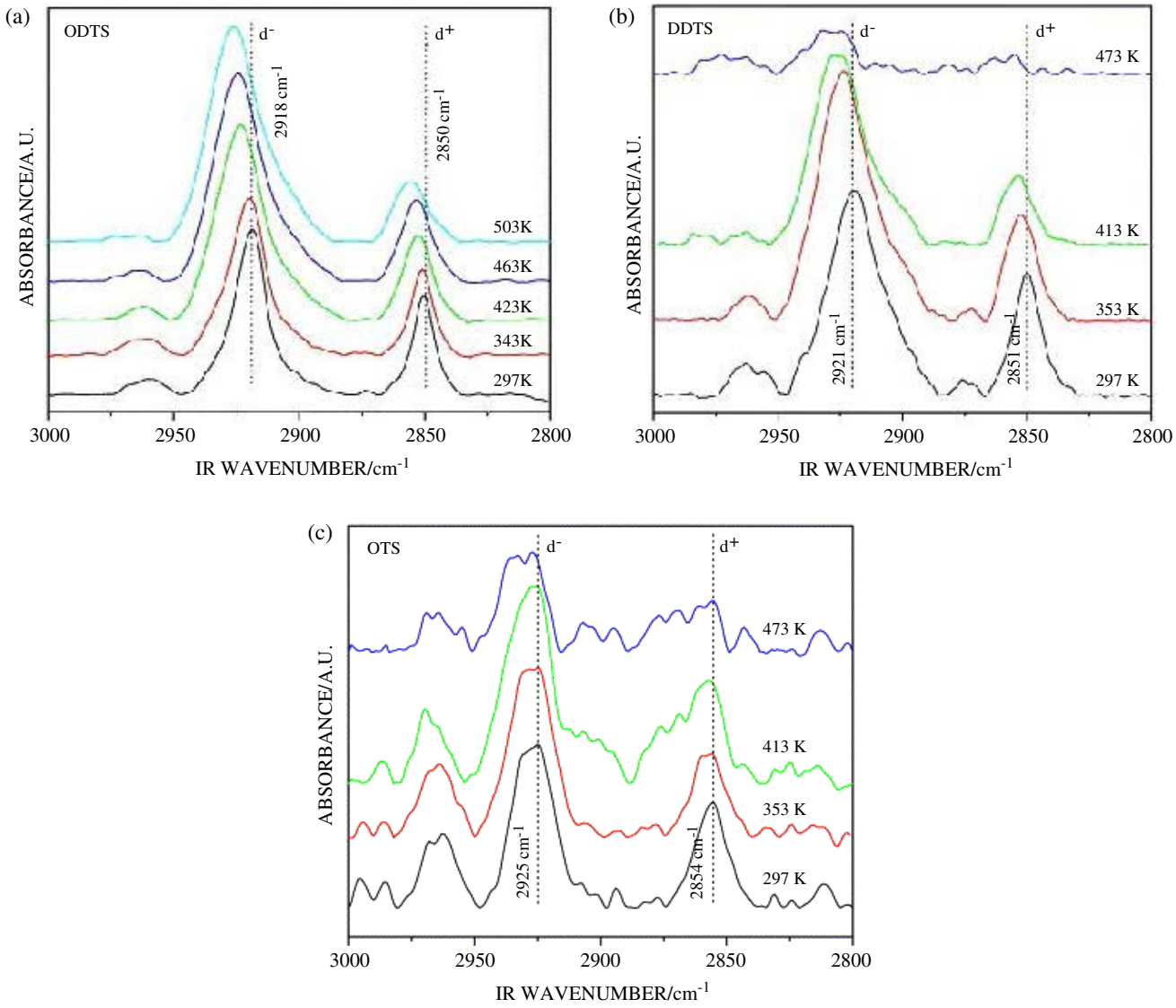

experiments of Salmeron[48–50] suggest that at high loads the load is borne by collective tilt and slipping of the molecules past each other. He argues that such a behaviour is possible when the molecules are tightly packed. When the molecules are less densely packed, space is available between the molecules for gauche defects to be generated down the backbone without causing too much steric hindrance. Thus, compression should generate significantly larger disorder in loosely packed molecules than in the more closely packed one, perhaps accounting for the larger friction generally observed in the former than in the latter.

When two surfaces slide against each other, the process is allowed to happen as they are kept pressed together by the normal load. To understand dissipation in the sliding process (which we argued earlier to be the most important physical process which accounts for the perpetuation of the friction force) it is therefore important for us to briefly supplement our experimentally obtained understanding of the consequence of normal load application by some elegant insights which have emerged from molecular dynamic simulation of the same process by Harrison and co workers[51–54].

In molecular dynamic simulation, the atoms in confinement are allowed to move freely according to classical dynamics. The equation of motion for all non-rigid atoms are integrated using a velocity

Figure 15: Temperature-dependent variations of fwhm of methylene antisymmetric stretch of ODTS monolayer for different thermal cycles. (■) heating of 270°C, (○) cooling from 270°C, (△) cooling from 210°C, and (□) cooling from 130°C. (b) Temperature-dependent variations of fwhm of mythylene antisymmetric stretch of alkylsilane monolayers, ODTS (■), DDTS (●), and OTS (▲), self-assembled on aluminum obtained for heating part of thermal cycles.

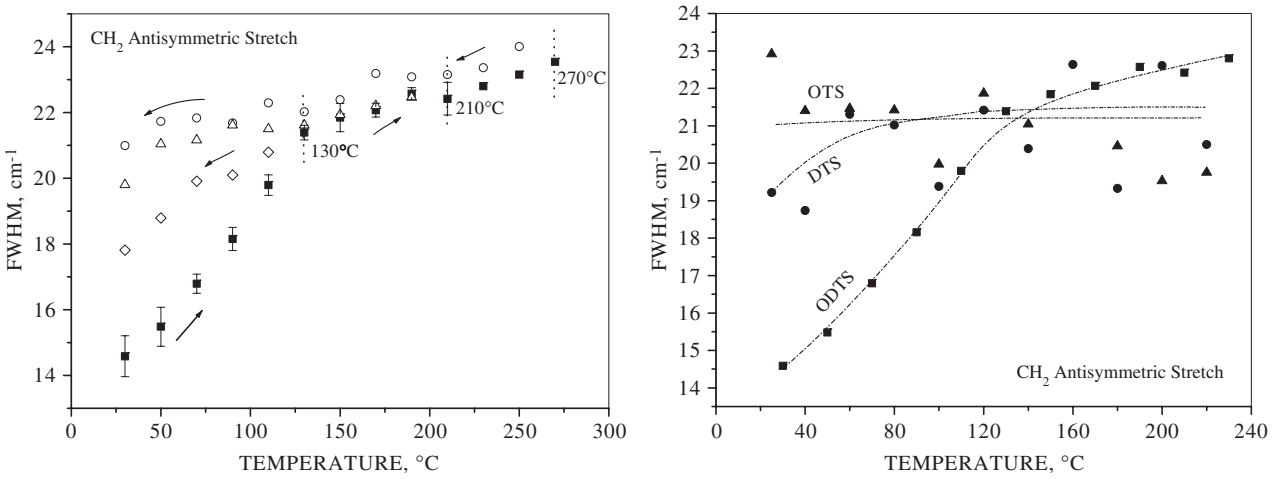

algorithm. The force on each atom is derived using a chosen potential.

Tutein et al.[52] considered linear hydrocarbon chains anchored to a semi infinite diamond plate being compressed by a semi infinite hydrogen terminated diamond plate. Gauche defects in this case are immediately generated at the terminal group level of the hydrocarbon, as was infact observed experimentally[48]. The confined molecules also tilt, and the tilt angle increases with the increasing load. On release of compression, the induced tilt disappears and the molecular axis springs back to its original position. As the load is applied and it increases with simulation time, the gauche defect population increases till it appears to reach saturation and remains constant with further increase in the load. It is never reduced to nil and in fact reaches a maximum when the load is reduced to nil. With time it reduces to nil, the time required for that being related to apriori defect population and temperature. It is important to note that the energy released when the molecules spring back on unloading is used to generate further gauche defect the population of which reaches maximum only when unloading is complete. There is thus always a phase lag. This is an important finding for tribology as will be discussed later. This phase lag generates a hysteresis observed in the difference in damping ability between the loading and unloading paths as seen in fig.13[47].

The situation does not change qualitatively when the flat compressor is replaced by a sharp indentor[51] except of course when the contact forces are much higher, there is penetration to great depths along the back bone because of much higher levels of local energy. There are some bond scissions. Molecules tilt in a less synchronized manner than in the case of flat compressor and perhaps the defect count per chain is high. The nature of increase in gauche defect count remains the same as in the

Figure 16: Plot of FWHM and initial coefficient of friction (μ_o) vs. heat treatment temperature for alkylsilane (ODTS, DDTS and OTS) monolayer deposited on aluminium. Values of FWHM were obtained from d^- stretch mode. Here block symbols are for FWHM and open symbols are for μ_o. There is a identical variation of FWHM and μ_o with heat treatment temperature for a particular monolayer system demonstrating a direct correlation between chain mobility and friction force.

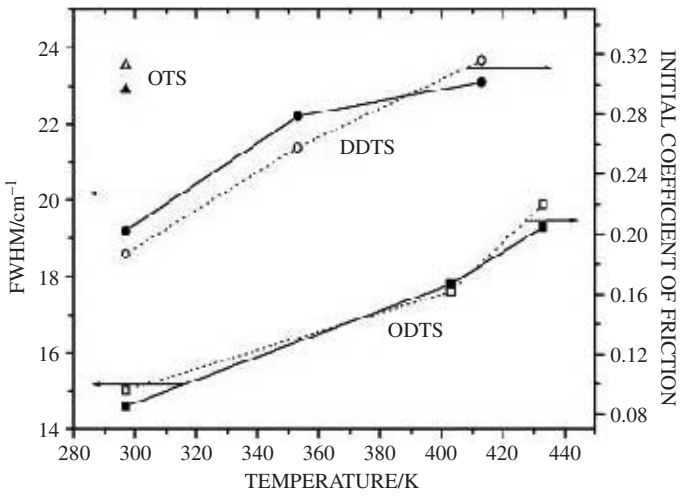

Figure 17: Plot of fwhm vs initial coefficient of friction (μ_o) for alkylsilane (ODS, DDTS and OTS) monolayers at different heat treatment temperatures. Values of fwhm were obtained from methylene antisymmetric (d^-) stretch mode. Here, μ_o shows a rough linear correlation with fwhm.

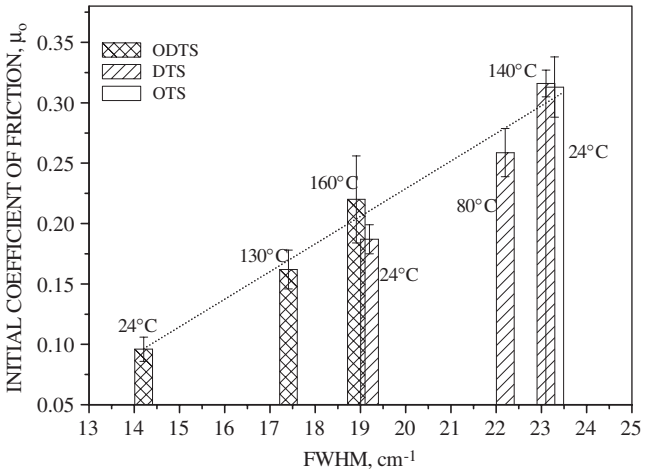

case of a flat compressor. The count increases with penetration and is independent of chain length in the C_{13}–C_{22} range. Comparing these results with the experimental finding (Salmeron's tips are of large radius as compared to those of Harrison) it is clear that the deformation becomes more synchronized and coherent as the tip geometry become increasingly flat.

Sliding Friction of SAM

To continue with the process simulation, Tutein et al.[52,51] shows that as the terminal end of a SAM molecule is pushed by the counterface in the sliding direction the friction force increases linearly. In this process the molecular length increases as it is stretched[53]. As the molecule is mechanically constrained, no gauche defects are generated during this phase; in fact, the defect count decreases. Once the molecule is released, it relaxes the stretching energy, which is utilized to generate gauche defects so much so that the when the stretching force is minimum the gauche defect count is maximum[52]. This is the avenue of energy dissipation. The higher the number of avenues of such dissipation higher is the amount of work which can be put into the system and higher therefore is friction. Combining this with the effect of pure normal compression[51] which shows the gauche defect population to increase with normal load, one would expect the friction force to increase with normal load. The relationship Mikulski and Harrison[54] demonstrate is almost linear at high loads though some anomaly related to packing density exists at low loads. They demonstrate quite clearly that due to the low steric constraint in a loosely packed monolayer the gauche defect generation is high and this results in higher friction. In a similar vain in a short chain monolayer low interchain Van-der-Waal force results in higher apriori defect population than is the case in a longer chain monolayer. The higher friction Tutein et al.[51,52] estimate therefore for the shorter chain monolayer, (the coefficient of friction appears to be the same) than in the longer chain monolayer is due to the higher level of apriori defect population in the shorter chain. Mikulski and Harrison[54] conclude that gauche defect may not be the principal causality of friction as torsional energy does plateau at a critical level of work input and they opine that the stretching mode is a good source of major energy dissipation.

To validate the above, we performed tribology[16−20] on three self assembled monolayers of the same chemistry but distinguished by their different packing density or available interchain spacing. We changed the packing density and disorder further by subjecting each species to heat treatment to different peak temperatures: Alkylsilane monolayers (octadecyltrichlorosilane (ODTS-C_{18}), dodecyltrichlorosilane (DDTS-C_{12}) and octyltrichlorosilane (OTS-C_8)) self assembled on pure (97.25%) aluminium surface were subject to heat-treatment cycles to peak temperature of 297 K, 253 K, 413 K, and 473 K. Figure 14 shows the representative vibrational spectra acquired by infrared reflection absorption spectroscopy (IRRAS). The figure shows the temperature dependent shifts of methylene antisymmteric (d^-) and symmetric (d^+) stretch modes. Figure 15 shows a summary of the full width half maximum FWHM data to indicate that decreasing the chain length and increasing the heat treatment peak temperature bring about pronounced reduction in the packing density of in these monolayers and crystallographic order in them. Figure 16 shows that decreasing the packing density increases the coefficient of friction (nanotribometer experiments using a steel ball[18]). Coupling the data presented in figs.15 and 16 shows (fig.17) that there is a linear increase in the coefficient of friction with a reduction in packing density. The contention which emerged from the experimental work of Salmeron and co-workers[48−50] and the molecular dynamic simulation work of Harrison and co workers[51−54] appears to be valid. Creation of greater free volume by a reduction of the packing density creates more avenues for rotation of molecular bonds and more frictional energy can thus be dissipated.

The MD simulation work quoted above clearly shows normal loading and tangential loading of

Figure 18: Coefficient of friction of ODTS monolayer self-assembled on silicon: load 100 mN, sliding velocity 0.02 cm/s, and 0% relative humidity. The monolayer is unloaded after different sliding times and rested for 10 min before being loaded again and the test recommenced. The figure shows the existence of a static friction obtained immediately on recommencement and a kinetic friction that changes perceptively with sliding time. It is to be noted that friction-time slope (θ) at interruption and recommencement of a test after prolonged stoppage (unloaded) are the same.

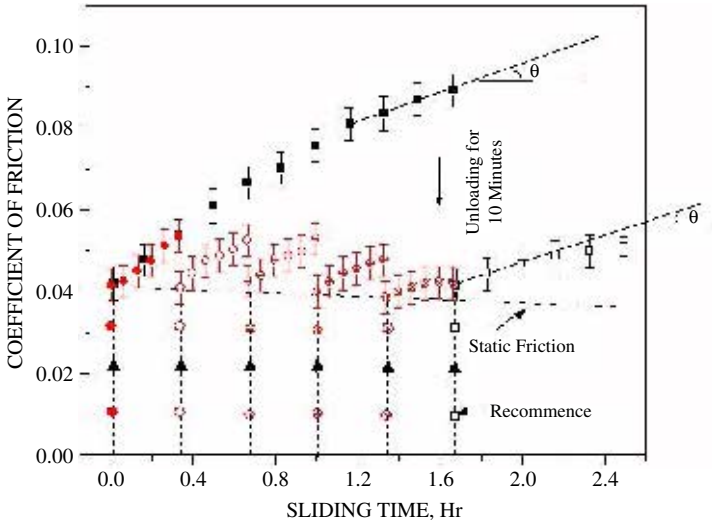

confined organic molecules to both generate gauche defects and cause stretching and bending of the chemical bonds. These deformations are reversible but have their characteristic life cycles which are not necessarily in phase with each other. In a real tribological situation microscopic events at the interface are more likely to be random than strictly periodic in time and space. For example, even if the SAM is strictly ordered the load on a molecule would vary and the time interval between collisions would vary from collision to collision depending on the spatial distribution of the asperities on the counterface and the substrate. The randomness is further enhanced if the molecules are disordered. Thus depending on the sliding velocity and load (we will demonstrate this effect later) the life of energy dissipating modes generated by normal and tangential loadings may not have the uniform wave like morphology in time predicted by the MD simulation[54]. It is of important to note at this stage the simulation work of Gao et al.[5] which predicts a similar space-time variation at the microscopic scale.

The above argument suggests that it is possible for a $0-0$ load life cycle of a dissipation mode to be interrupted by another collision event, the response to which would be modulated by apriori population of defects or a partially stretched bond. What this implies is that a time element, related to the periodicity of the collision events and the characteristics relaxation times of the dissipation modes, may play important roles in the tribology of organic SAMs. We will experimentally demonstrate below that this randomness does not get fully time averaged out into a time independent steady state average but manifests as an average friction which varies with time on a scale which is much larger than that for individual collisions. That friction varies with sliding velocity in certain regime of sliding velocity[7,9,4,14], with driving frequency and relaxation time[56,43] and with sliding time[55,4] have been observed. Yoshizawa et al.[4] in fact shows the friction to increase with a reducing slope with time to finally achieve a steady state value invariant with time.

Dissipation in intermittent tribological contact

In the experiments reported below a molecule is subjected to two types of intermittent contacts. When it is under the probe it is slid over the contact diameter. Line ($2\ \mu m$) scan of AFM topographical image of the steel ball ($2\times 2\ \mu m^2$ scan area) showed five asperities of height more than 1nm above a mean line. Taking these asperities as the contacting asperities, at the lower test velocity of 0.02 cm/s, a molecule is loaded by an asperity every 2×10^{-3}s. The time period ($t_r = \frac{(l-D)}{v}$) over which a molecule is not under the probe or the time which elapsed between its leaving a probe contact and the next probe contact is less than 1s at the lowest sliding velocity and 0.01 s at the highest test sliding velocity. The relaxation times τ_s, given in Table 1 show that of the two intermittency the one which gives the longer out of contact time is therefore the important one from the point of view of molecular relaxation. For the four different experimental conditions used here τ_s greater than t_r.

The experimental work of Salmeron and coworkers[40–42] shows that when an AFM tip slides over an organic monolayer gauche defects are generated at the terminal end of a molecule. When the molecule is released by the tip the defect relaxes back releasing frictional energy. Harrison and coworkers[51,54] using molecular dynamics simulation, show that in a single pass when a probe drags a molecule in the sliding direction, bonds stretch to increase the friction stress. When the molecule is released, it relaxes back to its original state. This is also supported by sum frequency generation spectroscopy[1,13] of mechanically compressed monolayer, which on unloading shows recovery but also some irreversible changes. In general, most previous works based on very short sliding distance experiments and

Figure 19: (a) Schematic showing a cycle of defect generation in a molecule as a function sliding. (b) Schematic showing accumulation of defect in a molecule with sliding time.

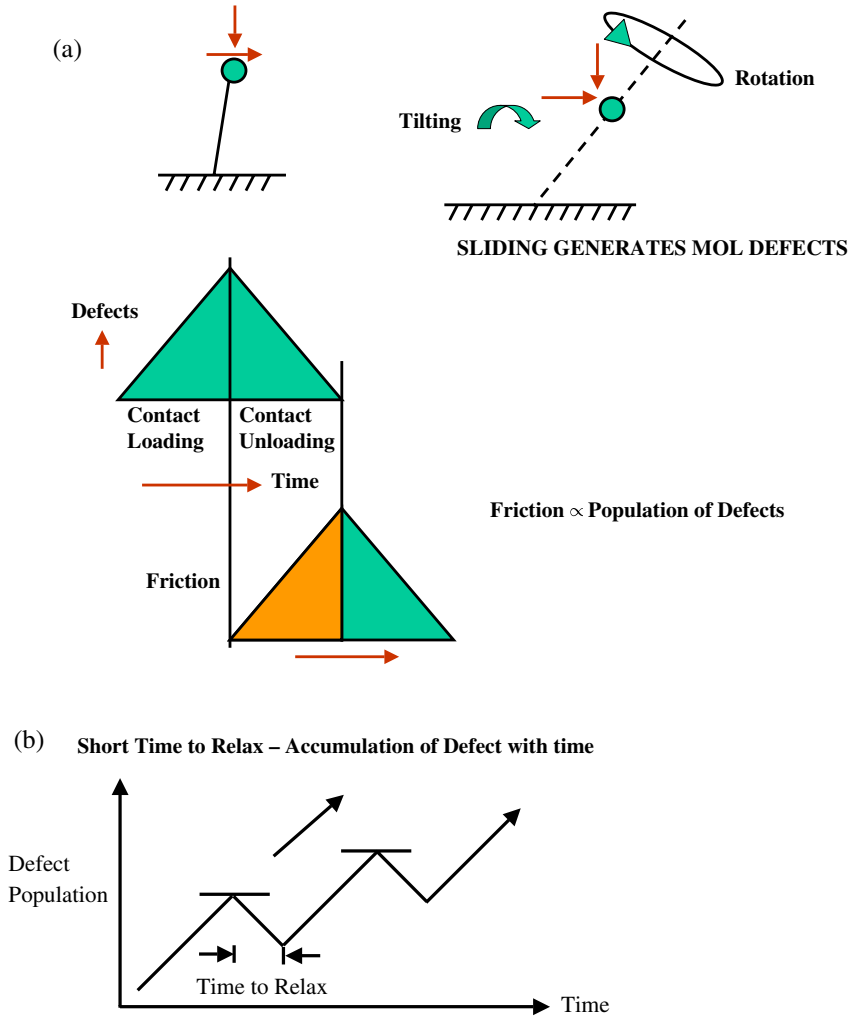

simulation suggest complete recovery of the original molecular structure on unloading. The complete recovery suggests that the characteristics relaxation time τ_s is less than or equal to t_r. In all these reported cases the friction rises to a peak between two contacts and falls back to the initial level before the next contact is made. The peak friction thus remains invariant over the complete duration of the sliding experiment.

In these[44] experiments a large number of molecules are in contact with the probe at any given time. As τ_s is greater than t_r, we may expect that the molecules do not have sufficient time to relax back before they come next into contact with the probe. They are thus likely to be able to relax the imposed strain only partially before the next contact. Thus the probe at the next contact meets residually strained molecules, with repeated contact the residual strain level can be expected to increase. If the state of strain by bond stretching or gauche defect generation are directly related to friction force as has been suggested, the friction force, as strains accumulate with repeated contact, can be expected to rise with time, as long as τ_s is greater than t_r.

Figure 18, shows the change in the coefficient of friction with sliding time measured in 0% RH environment at 0.02 cm/s velocity and 363 MPa mean contact pressure. Table 1 shows that under these experimental conditions, the value of τ_s is significantly greater than t_r. The friction is seen to increase with time. At the commencement of sliding, the friction force jumps to a certain value, which we designate as static friction, almost instantaneously. Static friction force needs to be reached before a kinetic friction regime is initiated where the friction increases gradually with time. The rate of rise of

Figure 20: (a) The effect normal load on coefficient of friction on ODTS monolayer, sliding velocity = 0.21 cm/s. (b) The effect sliding velocity on coefficient of friction on ODTS monolayer, normal load = 100 mN.

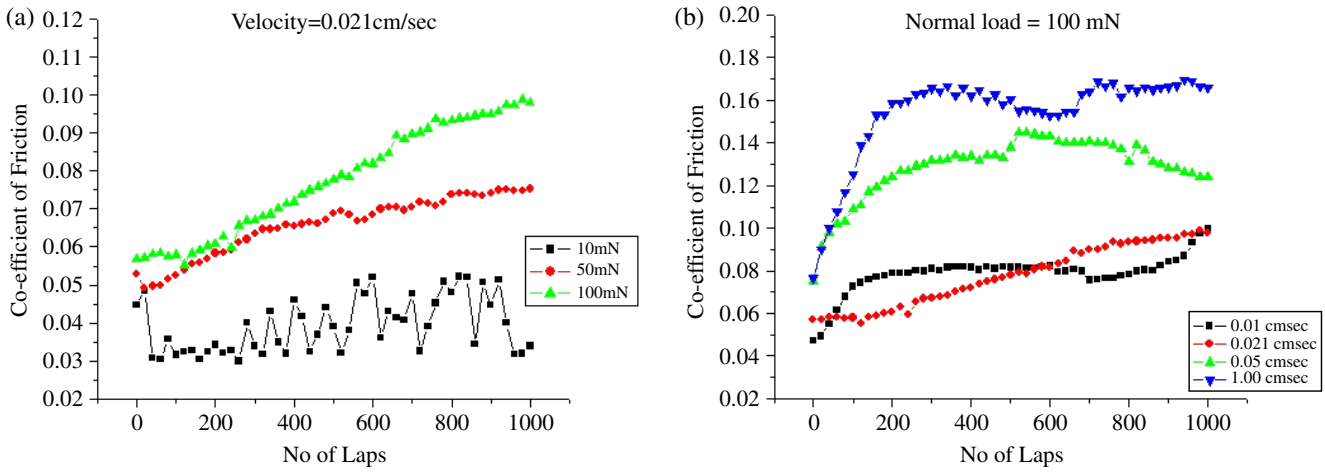

friction decreases with time till at large time when the friction becomes insensitive to sliding time. If the kinetic friction is assumed to be related to defect generation in sliding, it has been shown[43] that as defects accumulate it becomes more difficult to generate more defects.

When a test is interrupted, unloaded, stopped for a prolonged period of time and recommenced (loaded); the levels of static friction of an unslid ($t = 0$) monolayer is recovered initially; with increasing number of interruptions the recommenced static friction decreases slightly. The gradient of friction with time at recommencement however remains more or less the same as that at interruption. This is an important finding as it implies that it is possible to maintain a low level of friction with frequent interruptions.

Figure 21: Coefficient of friction of ODTS monolayer. The figure shows the effect of heat treating the monolayer apriori to 130°C peak temperature, before the commencement of sliding. Normal load:100 mN, sliding velocity: 0.02 cm/s.

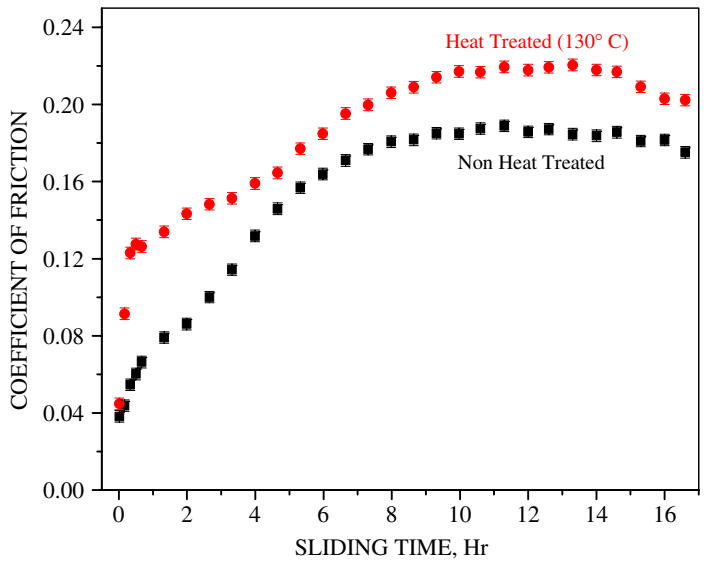

We may now combine the above observations to construct a simple model. Figure 19a shows an idealistic schematic where the population of defects or dissipation modes start to increase when the force experienced by the counterface asperity reaches its maximum and where the maximum work is done on the system. Figure 19b shows that if the time available (as dictated by a ratio of t_r/τ_s) to relax is not sufficient for the defects to decimate its population to nil, there is an accumulation of defects with each collision in that case.

If t_m is the time a group of molecules is in contact with a probe (assuming a contact diameter, D) in a cycle and $x\,t_m$ is the defect or strain generated during the contact, where x is a factor. Assuming relaxation is linear with time, the residual defect at the end of the cycle is given by:

$$\Delta g = \frac{\tau_s - t_r}{\tau_s} x t_m \qquad (5)$$

If t_r is the time a molecule is allowed to relax before the next contact,

$$t_m = \frac{D}{v}, \quad \text{where } v \text{ is the sliding velocity}$$

$$t_r = \frac{l - D}{v}, \quad \text{where } l \text{ is the stroke length.}$$

Figure 22: Effect of load on coefficient of friction (static) obtained on recommencement after a 10 min of unloaded rest. Sliding velocity: 0.02 m/s. The solid symbols represent continuous loading while the open symbols represent recommenced loading after interruption.

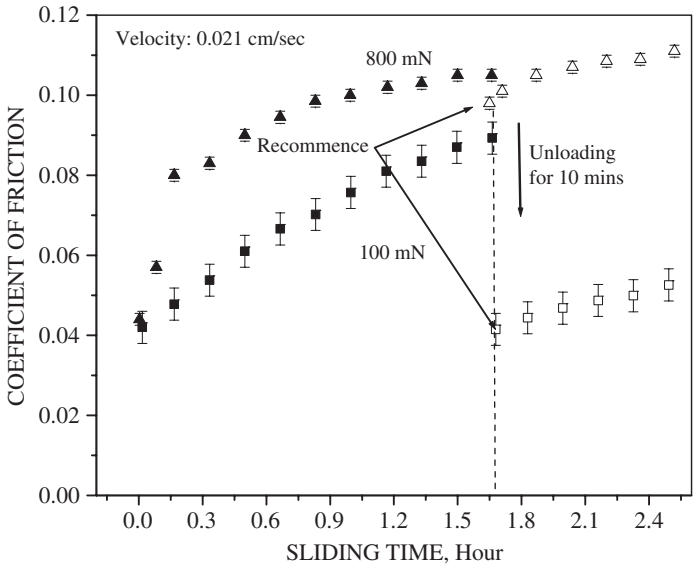

By taking that Δg is achieved in a cycle in time l/v, on substitution in eqn. (5) we get

$$\frac{dg}{dt} = \frac{xD}{l}\left[1 - \frac{l-D}{\tau_s v}\right] \tag{6}$$

If we now take that the defects saturate as more defects are generated, eqn. (6) becomes

$$\frac{dg}{dt} = \frac{xD}{lg^m}\left[1 - \frac{l-D}{\tau_s v}\right] \tag{7}$$

where g^m is a function of the current defect population, $1 > m > 0$.

If g_0 is the defect population at the commencement of the experiment, $(t = 0)$, we have

$$\int_{g_0}^{g} dg = \int_{0}^{t} \frac{xD}{g^m l}\left[1 - \frac{l-D}{\tau_s v}\right] dt$$

and

$$g = \left[g_0^{m+1} + \left\{\frac{(m+1)\,xD}{l}\left(1 - \frac{l-D}{\tau_s v}\right)t\right\}\right]^{\frac{1}{m+1}}. \tag{8}$$

The slope of the friction-time characteristic, as given by eqn. (7) for a given stroke length, l, is controlled by velocity v, τ_s and D. Note that τ_s and D are functions of the normal contact pressure. By varying the sliding velocity and normal load we can now manipulate dg/dt.

If we now assume that $\frac{df}{dt} \approx \frac{dg}{dt}$, the implications of the above model for friction are

1. If the sliding velocity is reduced, t_r increases and there is a corresponding reduction in $\frac{dg}{dt}$ and $\frac{df}{dt}$. Figures 20a and b show that the gradient of friction with time is greatly reduced and greatly enhanced when the sliding velocity is reduced from 0.02 cm/s to 0.001 cm/s. and increased from 0.02 cm/s to 1.05 cm/s, respectively.
2. If the normal load is increased, the relaxation time τ_s (fig. 12) and D are increased. According to eqn. (7) any such increase would increase $\frac{dg}{dt}$ and therefore overall level of friction as well.
3. Equation (6) shows the gauche defect count to increase with apriori population of the gauche defect. Figure 21 shows the friction with time of a heat treated monolayer to be much enhanced due to heat treatment. We have previously noted the effect of heat-treating a monolayer is to decrease its packing density.

Figure 18 indicates a complex response of organic self assembled molecules to sliding traction. We present below a possible simple model to account for the experimental observations. The frictional response of the monolayer is a composite of responses of two structurally distinct parts of a molecule. The stiff backbone is anchored chemically to the substrate and tightly bound with adjacent backbones by Van der Waal forces, the response of the backbone may be visualised as 'solid like' and elastic. The terminal end of the molecule has a large degree of freedom of movement and may be visualised as 'liquid like' and plastic. When the monolayer is slid, the backbone bends and stretches elastically until the terminal end yields marking a level of static friction. Once it yields, the terminal end becomes active and gauche defects are generated. In a cycle when the molecule is out of contact, the backbone is restored to its original state and the terminal end recovers partially, no doubt determined by the relative magnitude of τ_s and t_r. This is repeated with each cycle and the terminal end defects accumulate to yield a rising friction with time. When the experiment is stopped for a prolonged time, the elastic part of terminal defects has enough time to relax completely but some permanent strain is retained. When the test is recommenced after prolonged stoppage the SAM, by virtue of retention of some permanent defects at its terminal end, has a memory. This is reflected in the recommenced friction gradient after 'yield' being the same as that at

Figure 23: Difference between the coefficient of friction at interruption (kinetic friction) and that on recommencement (static friction) after 10 min unloaded rest, as a percentage of the coefficient of friction at interruption. There is little difference between the static and kinetic friction when the sliding distance is large. Load=800mN, velocity=0.02 cm/sec.

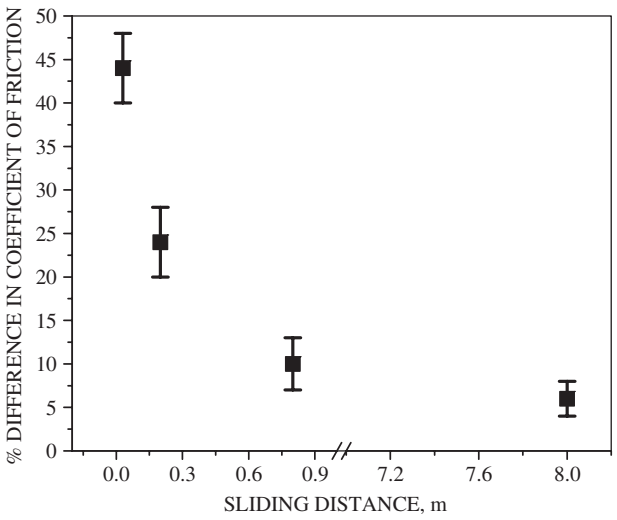

the time of interruption. With increasing number of interruptions the permanent defects at the terminal end accumulate. The increasing disorder softens the monolayer[56] and lowers the stress which marks static friction. Figure 18 shows this stress to decrease with increasing number of interruptions. When the normal load is increased, at large sliding times the immediate friction on recommencement (static friction) is much enhanced. Furthermore fig. 22 shows that this static friction approaches the kinetic friction registered at interruption. This possibly is due to the fact that at this high contact pressure regime, the response of the backbone to frictional stress is no longer elastic and it loses stiffness with time. Figure 23 shows the difference between kinetic (friction at interruption) and static friction (on recommencement after unloaded rest) reduce with time for a heavily loaded SAM.

It is important to note that the magnitude of the relaxation time which allows a positive friction-time gradient (which is experimentally observed) is several orders greater than what is expected for a single molecule[50]. As a matter of fact, if τ_m is the relaxation time of a single molecule and all the molecules in contact relax fully in time τ_m, when $\tau_m \lll t_r$, this gives $df/dt = 0$, which is of course contrary to experimental findings[44]. Overney[57] has shown that in efficient boundary lubrication, the molecules do not respond to traction individually but as constituents of a coherent volume. This cooperative behaviour lowers the activation energy barrier which needs to be overcome for sliding motion. The large relaxation times, which appear to be relevant to the tribological performance, suggest that the material response to traction should be tracked not on the basis of individual molecular behaviour but by recognizing an aggregate phenomenon which involves a large number of interacting molecules. This we believe is a phenomenon which may be unique for self assembled organic molecules which when collectively pressed are likely to interdigitise to minimise free volume. Such high values of relaxation time, in comparison to that of single molecules, have been observed in previous[45,47,58] experimental works on compression and shear of molecules in confinement.

Closure

The experiments reported as above point to the viscoelastic response of organic monolayers self assembled on solid surface. The molecular dynamic simulations clearly indicate that the rotational motion of the bonds continue well after unloading of the monolayer in compression and shear. The annealing of the molecules happen over a period of time. The rate at which this happens depends on the entropic state of the monolayer achieved on loading. Yoshizawa et al.[4] from SFA experiments, Garcia Parajo et al.[43] and Schonherr and Vansco[13] from the results of their AFM experiments, came to the conclusion that tribological interaction makes the monolayer disordered by interdigitation and entanglement. This takes the assembly to a state of relaxation times which are higher than that of the original monolayers and the force which are encountered in unloading are higher than on loading. Thus the monolayers on unloading has a time dependent viscous response. Yoshizawa et al (4) demonstrate that in moving from a crystalline to an entangled amorphous state, the frictional force is increased. They in fact show that the friction can be related to the hysterisis in a loading — unloading cycle. This view is supported by Schonherr et al.[13]. The work reported[44] shows that the process of full recovery, if that is possible, depending on the velocity and load, may be interrupted by the next collision. A partially recovered monolayer which is partially disordered and entangled is therefore taken to the next cycle of loading. It is inferred from the experimental data that this state of residual disorder accumulates with progressive sliding. As friction clearly scales with the state of disorder, the friction force, for a range of load and speed, increases with sliding time. If, for example, the latter parameters are such that the monolayer can recover completely, in a situation where complete

annealing is physically possible in a long period of rest, the friction force does not increase with sliding time. The reported work additionally shows that the rotational defect has two components: the recoverable and irrecoverable. The latter is retained even after prolonged rest at no load and influences the rate at which friction increases if a loaded interaction is recommenced. This indicates that an organic self assembled monolayer is capable of retaining a memory of past loading history. The results further point that the elastic loading of the backbone by stretching and bending happens almost instantaneously on loading. When the applied force reaches a critical load the terminal part of the monolayer 'melts' or 'yields' and this initiates the high energy torsional modes.

ACKNOWLEDGEMENTS

I am indebted to my research students, post doctoral fellows, Dr. R. Sahoo and Dr. O. P. Khatri, Mr. H. S. Shamsundar, Mr. S. R. Binu, Ms. Pushpa Raju and other incumbents of the laboratory for their contribution to the work which has made this essay possible. I am also grateful to the Centre for High Technology (Ministry of Petroleum, Govt. of India), General Motors (R&D), Warren, US and Indian Oil Corporation Limited (R&D) for their financial support for the works described in this review.

Received 23 January 2007; revised 26 February 2007.

References

1. Leslie, L, 1804, An experimental inquiry into the nature and propagation of heat, Bell and Bradfute, Edinburgh
2. Bowden, F.P., and Tabor, D. Friction and Lubrication of Solids, 1951(I), 1964(II), London, Oxford University Press.
3. Derjaguin, B.V. Z, Phys. 1934, 88, 661
4. Yoshizawa, H., Chen, Y., and Israelachrlli, J., J. Phys Chem 1993, 97, 4128–4140.
5. Gao, J., Luedtke, W.D., Gurdon, D., Ruths, M., Israelachrlli, J.N. and Landman, Uzi., J. Phys Chem. B. 2004, 108 (A), 3410–3425
6. Johnson, K.L., Kendall, K., and Roberts, A.D., Proc. Roy. Soc. London, 1971, A 324, 301
7. Liu, H, Ahmed, S.I and Scherge, M, Thin Solid Films, 2001, 381, 135–142
8. Ren, S, Yang, S and Zhao, Y, Langmuir, 2003, 19, 2763–2767
9. Ruths, M, Alcantar, N. A and Israekachvlli, J. N., J. Phys. Chem, 2003, 107, 11149 1157
10. Graupe, M., Koini, T., Kim, H.I., Garg, N., Miura, Y.F., Takanaga, M., Perry, S.S. and Lee, T.R., Mat. Res. Bull, 1999, 34(3), 447–453
11. Choi, J., Kawaguchi, M. and Kato, T., J of Applied Phys. 2002, 91(10), 2574–7576
12. Hayashi, K., Sugimura, H. and Takai, O., Jpn. J. Appl. Phys, 2001, 40 (Pt1), (6B), 4344–4348
13. Schonherr, H. and Vancso, G. J., Mat. Sc and Eng. C, 1999, 8-9, 243–249
14. Ishida, H., Koga, T, Morita, M, Otsuka, H, and Takahara, A. Trib. Lett., 2005, 19(1), 1–8
15. Zhang, L., Li, L. Chen, S. and Jiang, S., Langmuir, 2002, 18, 5441–5456
16. Devaprakasam, D., Khatri, O.P., Shankar, N., and Biswas, S.K, Tribology Int., 2005, 38, 1022–1034
17. Khatri, O.P. Devaprakasam. D. and Biswas S.K. Trib lett., 2005, 20 (3), 243–254
18. Khatri, O.P., Bain, C.D., and Biswas, S.K., J. Phys. Chem B, 2005, 109, 23405–23414
19. Khatri, O.P., and Biswas, S.K, Surface Science, 2006, 600, 4399–4404
20. Khatri, O.P., and Biswas, S.K, Surface Science, 2004, 572 (2-3), 228–238
21. D. Maugis, D., Contact, Adhesion and Rupture of Elastic Solids, 2000, Berlin, Springer-Verlag.
22. Ahn, H., Cuongo, P.D., Park, S., Kim, Y. and Lim, J., Wear, 2003, 255, 819–825
23. Sung, I.H., Yang, J.C., Kim, D., and Shin, B., Wear, 2003, 255, 808–818
24. Burnham, N.A., Domingnez, D.D., Mowery, R.L. and Colton, R.J., Phys. Rev. Lett, 1990, 64, 1931–1934
25. Takahara, A., Kojio, K. and Kajiyama, T., Ultramicroscopy, 2002, 91, 203–213
26. Koijo, K., Takahara, A. and Kajiyama, T., Langmuir, 2000, 16, 9314–9320.
27. Adhvaryu, A., Biresaw, G., Sharma, B.K. and Erhan, S.Z, Ind. Eng. Chem. Res, 2006, 45, 3735–3740
28. Kondo, H., Wear, 1997, 202, 149–153
29. Smith, O., Priest, M., Taylor, R.I., Price, R., Cantlay, A. and Mc Coy, R.C., Proc. I Mech E, Part J: J.Eng. Trib, 2006, 220, 181–189
30. St. Pierre, L.E., Owens, R.S. and Klint, R.V., Wear, 1966, 9, 160–168.
31. Porter, M.D., Bright, T.B., Allora, D.L. and Chidsey, E.E.D., J of Am. Chem. Soc, 1987, 109, 3559
32. Dubois, L.H., Zegarski, B.R. and Nuzzo, R.G., J of Chem. Phys. 1993, 98, 678
33. Bryant, M.A. and Pemberton, J.E., J. Am. Chem. Soc., 1991, 113, 8284
34. Fenter, P., Eisenberger, P., Burrows, P., Forrest and Liang, K.S., Physica, B., 1996, 221, 145
35. Fenter, P., Eisenberger, P. and Liang, K.S., Phys, Rev. Lett. 1993, 70, 2447
36. Wizrig, C.A., Chung, C. and Porter, M.D. J. Electroanal. Chem. 1991, 310, 335
37. Devaprakasam, D., Sampath. S. and Biswas, S.K., Langmuir, 2003, 20, 1329–1334
38. Hautman, J. and Klein, M.L. J. Chem. Phys. 1989, 91, 4994
39. Hautman, J., Bareman, J.P., Mar, W. and Klein, M.L., J. Chem. Soc. Faraday Trans., 1991, 87, 2031
40. Prathima, N., Harini, M., Rai, Neeraj Chandrashekara, R.H., Ayappa, K.G., Sampath, S. and Biswas, S.K., Langmuir, 2005, 21(6), 2364–2374
41. Bhatia, R. and Garrison, B.J., Langmuir, 1997, 13, 765
42. Benesebba, F., Ellis, T.M, Badia, M. and Lannox, R.B., Langmuir, 1998, 14, 2361
43. Garcia-Parajo, M., Longo, C., Servat, J., Gorostriza, P. and Sanz, F., Langmuir, 1997, 13, 2333–2339
44. Khatri, O.P. and Biswas, S.K., J. Phys. Chem. C, 2007, 111, 2696
45. Joyce, S.A., Thomas, R.C., Homston, J.E., Michalske T.A. and Crooks, R.M., Phys. Rev. Lett. 1992, 68, 2790
46. Jeffery, P.M., Hoffman, Pethica, J.B., Ramanujan, C., Ozger, H.O., and Oral, A., Phys. Rev. B, 2004, 70, 054114
47. Devaprakasam, D. and Biswas. S.K., Phys. Rev. B, 2005, 72, 125434
48. Salmeron, M. Trib. Letts, 2001, 10(1-2), 69–79
49. Lio, A., Morant, C., Ogletree, D.F and Salmeron, J. Phys. Chem. B, 1997, 101, 4767–4773
50. Barrena, E., Kopta, S., Ogletree, D.F. Charych, D.H., and Salmeron, M., Phys. Rev. Letts., 1999, 82, 14, 2880–2883
51. Tutein, A.B., Stuart, S.J. and Harrison, J.A., J. Phys. Chem, B, 1999, 103, 11357–11365

52. Tutein, A.B., Stuart, S.J., and Harrison, J.A, Langmuir, 2000, 16, 291–296
53. Mikulski, P.T and Harrison, J.A., Trib. Letts. 2001, 10(1-2), 29–35
54. Mikulski, P.T and Harrison, J.A. J. Am. Chem. Soc., 2001, 123, 6873–6881
55. Nakano, M., Ishida, T., Numata, T. Numata, T., Ando, Y. and Sasaki, Shinya, Jppn. J. Apl. Phys, 2003, 42, 4734–4738
56. Duwez, A.S., Jonas, U. and Klein, H., CHEM PHYS CHEM, 20 03, 4, 1101
57. Overney, R.M, Tyndall, G. and Formmer, J., Nanotechnology Handbook, Bhushan, B.Ed., Springer – Verlag, Heidelberg, Germany., 2004., Chapter 29
58. Demirel, A.L. and Granick, S., Phys. Rev. Letts., 1996, 77, 3261

Sanjay Kumar Biswas, after training in Engineering Mechanics during his PhD and postdoctoral work in UK, has been involved in research with different aspects of tribology. Presently he is a professor in Mechanical Engineering Department and Materials Research Centre in the Indian Institute of Science. His current interests are in nanomechanics and nanotribology. He is on the editorial boards of several international journals in tribology. He is also the co-founder of International Nanotribology Forum.